Original paper

Padrť Stock (Teplá–Barrandian Unit, Bohemian Massif): petrology, geochemistry, U–Pb zircon dating of granodiorite, and Re–Os age and origin of related molybdenite mineralization

Karel ŽÁK[1]*, Martin SVOJTKA[1], Karel BREITER[1], Lukáš ACKERMAN[1], Jiří ZACHARIÁŠ[2], Jan PAŠAVA[3], František VESELOVSKÝ[3], Jiří LITOCHLEB[4†], Jana ĎURIŠOVÁ[1], Eva HALUZOVÁ[1,2]

[1] *Institute of Geology AS CR, v.v.i., Rozvojová 269, 165 00 Prague 6, Czech Republic; zak@gli.cas.cz*
[2] *Institute of Geochemistry, Mineralogy and Mineral Resources, Faculty of Science, Charles University in Prague, Albertov 6, 128 43 Prague 2, Czech Republic*
[3] *Czech Geological Survey, Klárov 3, 118 21 Prague 1, Czech Republic*
[4] *National Museum, Václavské náměstí 68, 115 79 Prague 1, Czech Republic*
**Corresponding author*
[†] *Deceased*

The Padrť Stock is a small (~5 km^2) intrusion located near the SE margin of the Teplá–Barrandian Unit, Bohemian Massif, several kilometers away from the NW periphery of the Central Bohemian Plutonic Complex. On outcrops, which are all located close to the contact of the stock with Neoproterozoic sedimentary rocks, two types of granitoids were detected, fine- to medium-grained hornblende–biotite Padrť granodiorite, and, along its SW margin, fine- to medium-grained partly porphyritic biotite Teslíny leucogranite. The U–Pb zircon dating of the more voluminous Padrť granodiorite by laser ablation ICP-MS yielded a magmatic age of 342.8 ± 1.1 Ma, which is slightly lower than are the published age data for the nearby Blatná suite granitoids of the Central Bohemian Plutonic Complex. The Re–Os dating of molybdenite occurring in quartz veins within a quartzite lens in close exocontact yielded ages of 337.2 ± 2.4 Ma and 339.8 ± 2.5 Ma (two samples). The data indicate that the formation of molybdenite postdated that of the magmatic rock. This is in agreement with relatively low-temperature deposition of quartz related to formation of the molybdenite, as indicated by the fluid inclusions (280 to 300 °C).

Keywords: Teplá–Barrandian Unit, Variscan granitoids, petrology, geochemistry, U–Pb zircon dating, Re–Os molybdenite dating
Received: 27 February 2014; accepted: 21 October 2014; handling editor: J. Žák
The online version of this article (doi: 10.3190/jgeosci.177) contains supplementary electronic material.

1. Introduction

Several small stock-like granitoid intrusions occur at the SE rim of the Teplá–Barrandian Unit (TBU). The Bohutín Stock (~3.4 km^2 at the surface; Dudek and Fediuk 1956; Vlašímský 1982; Bambas 1990) is dominated by quartz diorite and granodiorite. It is, thanks to underground mining of Ag–Pb–Zn–Sb vein-type ores of the Bohutín Deposit (Piša 1966; main operation 1841–1979), documented down to a depth of 1.350 m below the surface. Another intrusive stock in this area is represented by the poorly known Padrť Stock, located farther to the W (see Fig. 1).

All these small intrusions belong to the NW peripheral part of the Příbram Ore Region, an area exploited for vein-type ores and geologically studied for centuries (e.g., Bambas 1990; Žák K and Dobeš 1991). These small stocks intruded almost unmetamorphosed Neoproterozoic and Cambrian sedimentary rocks at a distance of several km away from the Central Bohemian Plutonic Complex (CBPC). The CBPC is a voluminous multiphase intrusive complex (*c.* 3.200 km^2; Holub et al. 1997b), which is well characterized with respect to petrology, geochemistry and ages of individual intrusions (e.g., Janoušek et al. 1995; Holub et al. 1995, 1997a; Janoušek et al. 2000a, 2000b, 2004, 2010; Žák J et al. 2005a, b, 2009). The ages of the main-phase plutons within the CBPC range from 354 ± 4 Ma to 337 ± 1 Ma. Deeper within the TBU and another 25 km to the W, small early-Variscan Štěnovice Pluton (~27 km^2, granodiorite–tonalite) occurs, for which zircon U–Pb dating yielded an age of 375 ± 2 Ma (Žák J et al. 2010).

The Padrť Stock is little known due to its location inside the Brdy Military Training Area with restricted access (1927–recent) and because it is largely concealed beneath Quaternary cover. Rather controversial views regarding the petrology and extent of the Padrť Stock were presented in the geological maps and short papers (e.g., Fediuk 2008). The purpose of this study is not only to bring new petrological and geochemical insights, but also provide U–Pb age for the Padrť Stock. The research focused also on sub-economic molybdenite mineralization in quartz veins within a thermally-metamorphosed quartzite at its exocontact. Lastly, in order to improve the

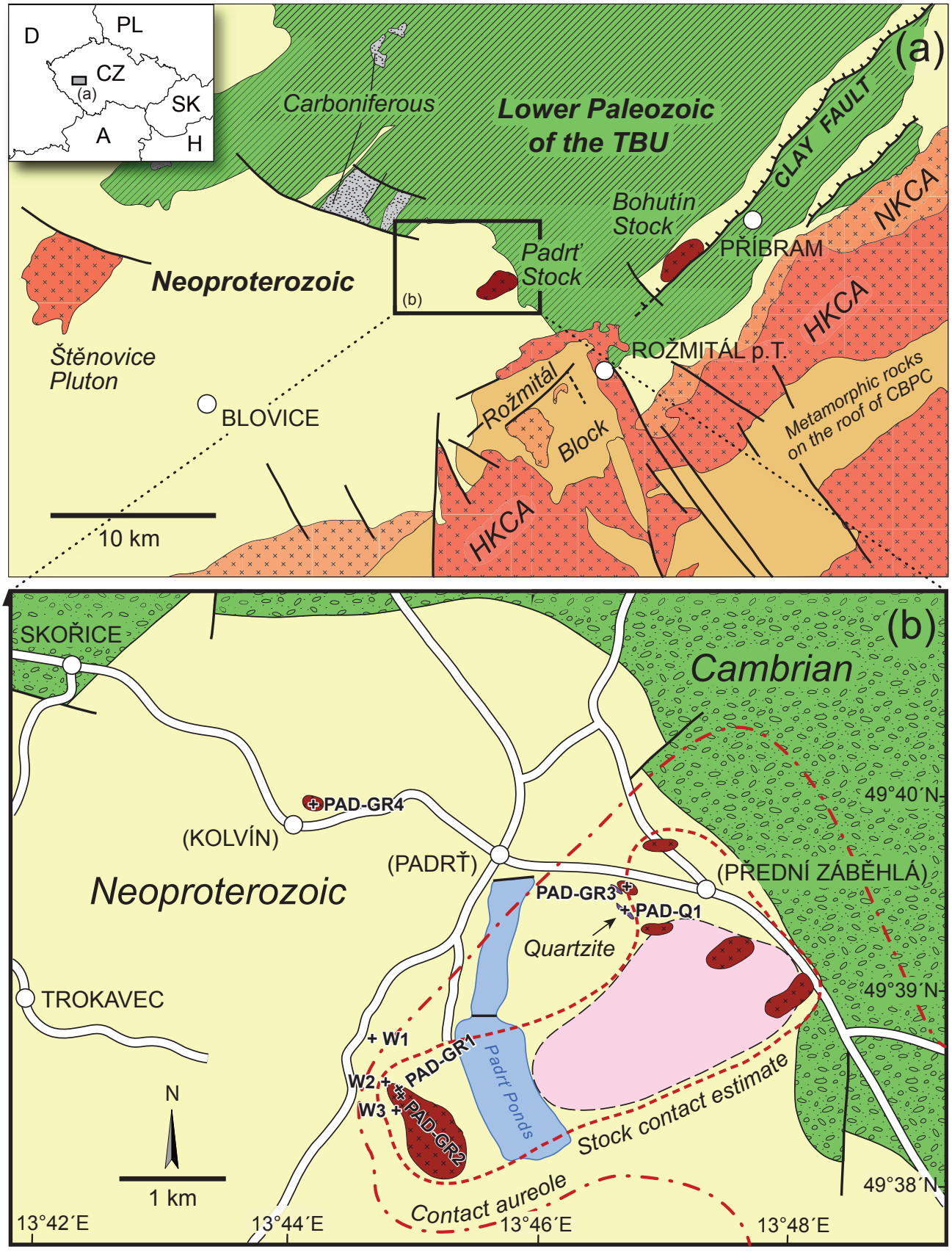
D
PL
CZ
(a)
SK
A
H
(a)
Carboniferous
Lower Paleozoic of the TBU
CLAY FAULT
NKCA
Bohutín Stock
PŘÍBRAM
Padrť Stock
(b)
Neoproterozoic
HKCA
ROŽMITÁL p.T.
Štěnovice Pluton
BLOVICE
Rožmitál Block
Metamorphic rocks on the roof of CBPC
10 km
(b)
SKOŘICE
Cambrian
PAD-GR4
(KOLVÍN)
(PADRŤ)
(PŘEDNÍ ZÁBĚHLÁ)
49°40´N
Neoproterozoic
PAD-GR3
PAD-Q1
Quartzite
TROKAVEC
49°39´N
+ W1
W2 +
W3 +
PAD-GR1
PAD-GR2
Padrť Ponds
Stock contact estimate
N
1 km
Contact aureole
49°38´N
13°42´E
13°44´E
13°46´E
13°48´E

understanding of relationships between the Padrť Stock and the molybdenite mineralization, fluid inclusions from three quartz types were studied and molybdenite dated by the Re–Os method.

2. Geological setting

2.1. Regional position of the Padrť Stock and studied samples

The Padrť Stock (Fig. 1a–b) is located close to the SE margin of the TBU, where several sets of regional faults intersect. Into the area south of Padrť, there is directed the SW continuation of the NE–SW oriented, regionally important fault system of the so-called Clay Fault. The Clay Fault is, at the current exposure level, responsible for repetition of belts of Neoproterozoic and Cambrian rocks, and it also controls the extent of the Ag–Pb–Zn veins in the Příbram Ore Region. Younger phases of movement on this tectonic zone are visible as faults inside the Bohutín Stock, but the displacement was small, on the order of 20 m at maximum (Bambas 1990). The main phases of movements on this fault system therefore pre-dated the intrusion of the Bohutín Stock and the formation of vein sulfidic mineralizations. Minor movements probably continued until the Tertiary (see Knížek 2013).

South of the Padrť area is located the Rožmitál Block, a relic of the contact-metamorphosed roof of the CBPC. It contains Cambrian to Devonian metasedimentary rocks intruded by granitoids with Au mineralization (Yazdi 1997; Yazdi et al. 1997; Zachariáš et al. 2001). The Rožmitál Block is surrounded by granite intrusions of the Blatná suite; its boundaries are locally modified by faults. The faults of NW–SE direction partly limiting the Rožmitál Block on its eastern side are also directed into the Padrť area, where they can be responsible for the boundary between the Neoproterozoic and Cambrian sediments.

The Padrť depression is limited on its eastern and northern sides by steep slopes with outcropping Cambrian continental clastic sedimentary rocks – predominating quartz-rich conglomerate with minor greywackes, quartz sandstones to quartzites. The Padrť Stock itself intruded shale and greywacke with lenses of silicites and bodies of submarine basaltoids, i.e. a rock sequence typical of the Blovice Complex of the TBU (Hajná et al. 2011).

The real extent of the Padrť Stock is not precisely known. There are only a few drillings (two of them were discussed by Fediuk 2008) and the rest of knowledge comes from rare outcrops and/or loose granodiorite blocks. Figure 1b shows the extent of the Padrť Stock in geological map 1:200 000 (Čepek and Zoubek 1961). In the granodiorite area shown on this map, the current authors were able to find only several weathered granodiorite blocks contained in the Quaternary cover and grus in the dumps of an abandoned 19th century Fe mine.

2.2. Contact-metamorphosed rocks and ore mineralizations

Manifestations of contact metamorphism by both Bohutín and Padrť stocks can be typically found up to several hundred meters from the contact, but never more than 1 km away (Bambas 1990). Apart from the common types of Neoproterozoic contact-metamorphosed rocks, several others can be found at the exocontact of the Padrť Stock. One of them is a graphite-rich chiastolite slate (with ~4.2 wt. % C), which was found in now inaccessible draining gallery of the Fe mine located near the eastern contact of the Padrť Stock. The chiastolite slate probably represents a tectonic segment within the fault zone bordering also the Cambrian sediments. This rock was identified by Slavík (1915), who, based on similarities to other contact-metamorphosed rocks in the area of CBPC, considered its precursor to be Ordovician shale.

Two lenses of light-gray to almost white, fine-grained quartzite occur very close to the contact of the Padrť Stock SW of the former village of Přední Záběhlá (Ambrož 1865). They are not shown properly on the published geological maps. Except for abundant arsenopyrite both contain also other interesting ore minerals; in one of the lenses molybdenite occurs as large flakes (up to 5 mm across) in quartz veins and partly also in the host quartzite. The second quartzite lens was described to contain antimonite mineralization (Ambrož 1865), which the authors have not been able to confirm.

3. Analytical methods

3.1. Sampling

All sites where granitoids were sampled are located outside of the extent of the Padrť Stock shown on the

⇦

Fig. 1 Location of the studied area and sampling sites. **a** – Geological sketch of the boundary zone between the TBU and CBPC, based on geological map of Čepek and Zoubek (1961); granitoids: NKCA – normal-K calc-alkaline (Sázava suite), HKCA – high-K calc-alkaline (Blatná suite); A – Austria, CZ – Czech Republic, D – Germany, H – Hungary, PL – Poland, SK – Slovakia. **b** – Detailed map of the study area with position of studied samples. The extent of the Padrť Stock after Čepek and Zoubek (1961) is shown in light color (see the stock shape in the part (a) of the figure); the areas where outcrops or at least isolated blocks of granitoids were documented by the authors are in darker color and hatched. Positions of drillings W1, W2, and W3 discussed by Fediuk (2008) are also included. The ruins of the former Teslíny Monastery are located between the drillings W2 and W3.

published geological map of Čepek and Zoubek (1961). The best outcrops, described in detail already by Ambrož (1865), are located proximally north of the ruins of the former Teslíny Monastery (samples PAD-GR1, PAD-GR2; Teslíny means always the ruins of the former small monastery in this paper, not the village of the same name located more to the south). These outcrops became later forgotten and are not shown on any modern geological maps. The drillings described by Fediuk (2008) are located close to this area. The second sampled site is represented by blocky outcrops close to the former village Přední Záběhlá (PAD-GR3). The third site where granitic rocks were sampled is an outcrop of a very small, probably isolated stock (~60 m in diameter) in an abandoned pit for quarrying granodiorite grus in the former village Kolvín (PAD-GR4). This granodiorite body, outcropping as large blocks at the bottom of this pit, was never mentioned or mapped before. Therefore, this site represents a new field discovery (first identified by J. Litochleb), located deeper inside the TBU at a distance of 4 km away from the earlier known outcrops of granitoids. All samples of granitoids were taken in the field from internal parts of large (0.5 to 1.0 m) blocks.

The quartz veins containing molybdenite were sampled for Re–Os dating and for fluid inclusion study. Positions of samples are shown in Fig. 1b.

3.2. Whole-rock and mineral chemistry

After homogenization, whole-rock major- and trace-element analyses were carried out in laboratories of the Czech Geological Survey (V. Janovská and R. Kašičková analysts). Silica was determined using titration method. Other major oxides were measured using Flame Atomic Absorption Spectroscopy on an AAnalyst 100 instrument. Analytical errors for major-element analyses in this laboratory were discussed in detail by Dempírová (2010) and Dempírová et al. (2010). Carbon and sulfur were determined on an element analyzer ELTRA CS-500, which measures the C and S content of the gasses produced by sample combustion using infrared absorption. Trace elements were determined by the X-ray fluorescence method on an ARL9400 Advant´XP instrument. The precision of the analyses varied between 1 and 5 %, depending on the elemental concentration (detection limits were 1–2 ppm).

Rock-forming silicate minerals were analyzed using a CAMECA SX100 electron microprobe at the Institute of Geology of the Academy of Sciences of the Czech Republic (AS CR), Prague, in wavelength dispersive mode, using an accelerating voltage of 15 kV, beam current of 10 nA, and a beam diameter of 2 μm. The following standards and X-ray K_α lines were used: Na, Al – jadeite, Mg, Si, Ca – diopside, K – leucite, Ti – rutile, Ba – baryte, P – apatite, Mn – $MnCr_2O_4$, Fe – magnetite, and F – fluorite.

The peak counting times were (in seconds), F 30, Na 20, Si 10, Mg 10, Al 10, K 10, Ca 10, Ti 20, Mn 30, Fe 30, Rb 30, Ba 10, Cr 30, Cs 30, Zn 6. The raw data obtained from electron microprobe were reduced using X-Phi(ZAF) procedure (Merlet 1994).

3.3. U–Pb dating of zircons

Zircon grains were separated from the fresh rock sample using conventional techniques: crushing, Wilfley concentration table, and finally, magnetic and heavy liquid separations (tetrabromoethane, density of *c.* 3 g . cm^{-3}, and diiodomethane). After that, zircon concentrates were handpicked for morphological types and mounted in an one-inch epoxy disc and polished. Before analysis in the mass spectrometer, the internal zircon structures and inclusions were characterized by backscattered electron (BSE) and cathodoluminescence (CL) imaging using a Tescan scanning electron microscope at the Institute of Geology AS CR, Prague.

The Pb/U isotopic ratios were acquired using an Element 2 (Thermo Scientific) high-resolution sector field mass spectrometer coupled with a 213-nm NdYAG UP-213 laser ablation system (New Wave Research), housed at the Institute of Geology AS CR, Prague. Samples were ablated in an original New Wave Research large format ablation cell. The laser was fired at a repetition rate of 5 Hz, using a spot size of 30 μm and a fluence of *c.* 9 J/cm^2. Acquisitions for all measured samples consisted of a 35 s measurement of blank followed by acqusition of U and Pb signals from zircons for another 60 s. Data were collected for masses 204, 206, 207, 208, 232 and 238 using both analogue and ion counting modes of the SEM detector, one point per mass peak and relevant dwell times per mass of 10, 15, 30, 10, 10 and 15 ms. The sample introduction system was modified using Y-piece tube attached to the back end of the plasma torch and connected to the helium gas line carrying the sample from the laser cell. The Hg impurity in the carrier He gas, which can cause isobaric interference of ^{204}Hg on ^{204}Pb, was reduced by using in-house made gold-coated sand trap. The relative contribution of common Pb to total Pb was less than 0.1 % and, therefore, no common Pb correction was applied to the data. Elemental fractionation and instrumental mass bias were corrected by normalization of internal U–Pb calibration zircon standard 91500 (1065 Ma, Wiedenbeck et al. 1995) and reference natural zircon standard GJ-1 (609 Ma, Jackson et al. 2004) periodically analyzed during the measurement for quality control. The obtained concordia ages of these standards 1062 ± 5 and 610 ± 3 Ma (2σ) correspond well within the errors to published zircon standards ages. Raw data reduction and age calculations, including corrections for baseline, instru-

mental drift, mass bias and down-hole fractionation, were carried out using the computer programs Iolite (Paton et al. 2010, 2011) and Isoplot (Ludwig 2003).

3.4. Re–Os molybdenite geochronology

The Re–Os molybdenite dating was also performed at the Institute of Geology AS CR, Prague, using the Re spike–Os normal method (Selby and Creaser 2001). A detailed description of the analytical procedure (sample decomposition, Re–Os separation), including preparation and calibration of the ^{185}Re spike–Os normal solution, was given elsewhere (Kohút et al. 2013). Rhenium concentrations were determined using multi-collector inductively-coupled plasma mass spectrometry (MC-ICPMS) on *Neptune* (Thermo Scientific) at the Czech Geological Survey, Prague. The instrument was coupled with a desolvation nebulizer Aridus II (CETAC) to achieve a more stable signal. The isotopic fractionation was corrected online using exponential law and Ir as an internal standard added to measured Re analyte solutions (Schoenberg et al. 2000; Li et al. 2010). An ^{191}Ir/^{193}Ir value of 0.594184 (Walczyk and Heumann 1993) was employed for mass bias correction. Six Faraday cups were used for simultaneous detection of ^{185}Re (L2), ^{186}W (L1), ^{187}Re (C), ^{190}Os (H1), ^{191}Ir (H2) and ^{193}Ir (H3). ^{190}Os was monitored to check possible Os interference on Re; however, no Os signal above background was observed confirming the effectiveness of the Re–Os separation procedure. In-run precision (relative standard deviation) of Re isotopic ratio measurements was better than ±0.02 % (2σ). Osmium isotopic composition was analyzed as OsO_3^- using a Finnigan MAT 262 thermal ionization mass spectrometer (N-TIMS; Creaser et al. 1991; Völkening et al. 1991) at the Czech Geological Survey following the methods outlined in Kohút et al. (2013). Internal precision (relative standard deviation) for ^{187}Os/^{188}Os determination in this study was ±0.03 % (2σ). The total procedural blank was 0.1 pg for Os with ^{187}Os/^{188}Os of 0.7±0.1 and 5 pg for Re. The accuracy of the Re–Os method was monitored through the analyses of NIST 8599 Henderson mine molybdenite reference material (Markey et al. 2007). Total analytical uncertainties (2σ) for all Re–Os ages include propagated uncertainties arising from Re and Os isotopic measurements, Re spike–Os normal solution calibration, blank correction and the error on ^{187}Re decay constant of Smoliar et al. (1996).

3.5. Fluid-inclusion study

Fluid inclusions were studied at the Faculty of Science, Charles University in Prague, using Leica DMPL and Olympus BX-40 microscopes and a Linkam THMSG 600 heating–freezing stage. Salinity of aqueous-only inclusions was calculated using the equation of Bodnar (1993). Salinity of aqueous–carbonic inclusions was estimated using software of Bakker (1997). Bulk composition and fluid isochores were computed using equation of state (Bakker 1999) implemented in the software FLUIDS (Bakker 2003).

4. Results

4.1. Petrology and geochemistry

Samples of granitoids from the studied Padrť area include two distinctly different facies: hornblende–biotite granodiorite and biotite leucogranite (Fig. 2).

Dark gray fine-grained weakly porphyritic hornblende–biotite granodiorite was found in blocky outcrops near the former Teslíny Monastery (PAD-GR2) and near the former village of Přední Zaběhlá (PAD-GR3). A non-porphyritic, very fine-grained variety of the same granodiorite crops out in a small abandoned sandpit in the former village of Kolvín (PAD-GR4). Both varieties of the granodiorite are composed of about 30–31 vol. % quartz, 33–37 % plagioclase, 8–11 % K-feldspar, 14–15 % biotite and 8–11 % actinolitic hornblende. Apatite, zircon and pyrite are accessory phases.

Mostly subhedral plagioclase is zoned with cores of $An_{0.35–0.40}$ (andesine) and rims $An_{20–30}$ (oligoclase). Younger anhedral and perthitic K-feldspar contains 0.3 to 1.1 wt. % BaO (0.005 to 0.020 apfu Ba). Abundant subhedral hornblende (Mg-hornblende to actinolite) forms clots together with biotite. Hornblende is homogeneous or only insignificantly zoned with Mg# (Mg/(Mg + Fe)) in the range 0.50–0.55. At Kolvín, the Mg# reaches up to 0.72. Hornblende is generally Si-rich (mostly in the range 7.4–7.9 Si apfu; Fig. 3; Electronic Supplement 1). Biotite (annite) which was later than hornblende, is chemically homogeneous (Mg# = 0.40–0.45: Fig. 4; Electronic Supplement 2).

Light gray to whitish fine-grained weakly porphyritic biotite leucogranite has been found in several blocks near the former Teslíny Monastery (PAD-GR1). It is composed of approximately 37 vol. % quartz, 30 % oligoclase–andesine ($An_{18–34}$), 28 % K-feldspar, and 5 % biotite. Apatite and zircon represent accessory phases. Perthitic cores of the K-feldspar grains are enriched in Ba (up to 0.65 wt. % BaO) compared to the rims (<0.1 wt. % BaO). Annite (Mg# = 40–41) is the only mafic mineral.

The chemical compositions of both rock types are summarized in Tab. 1 and the relationships between some chemical elements plotted in Fig. 2. Comparisons of the chemistry of hornblende and biotite from the studied rocks to the compositions of the same minerals in granitoids of the CBPC are made in Figs 3 and 4.

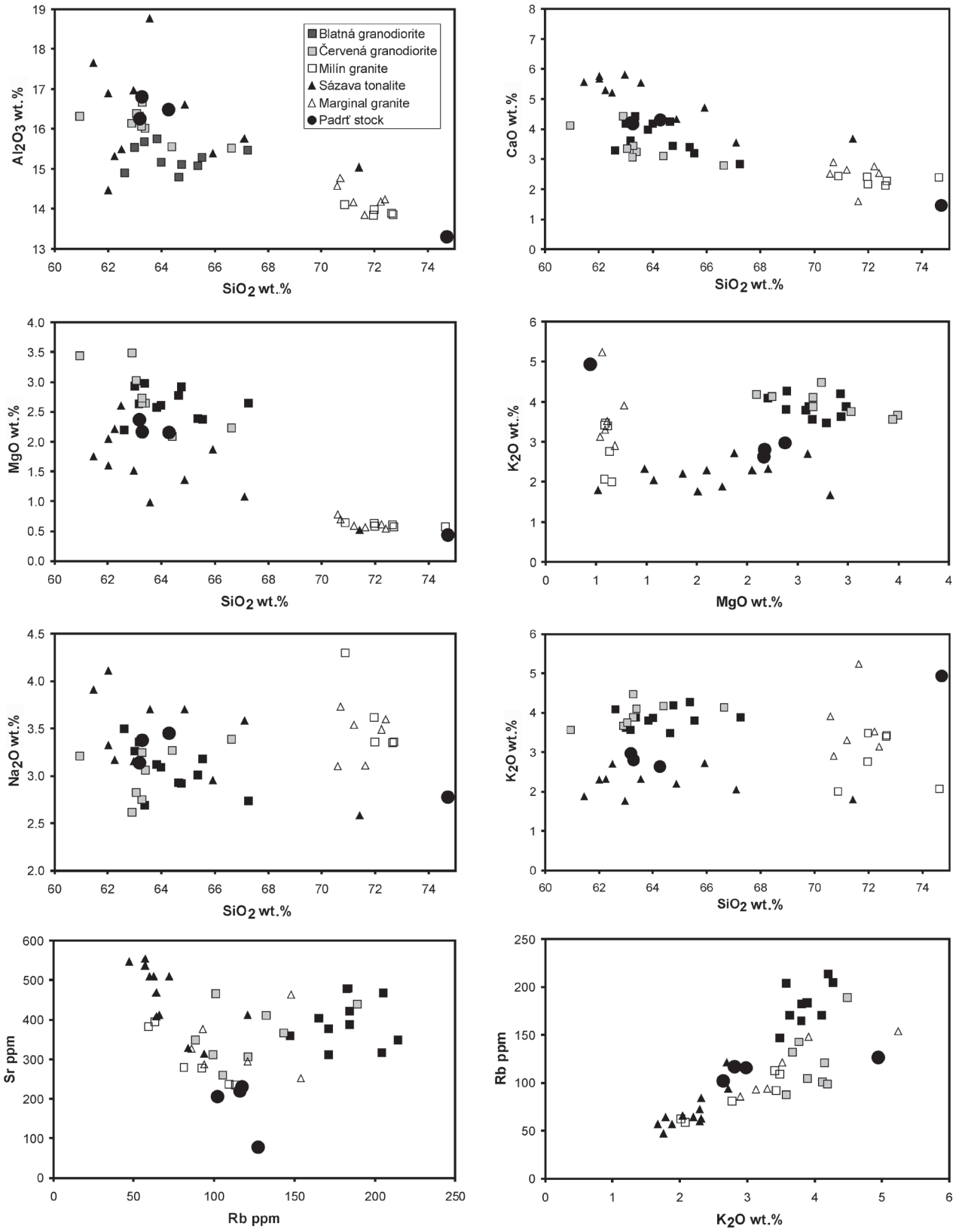

Fig. 2 Comparison of chemical composition of Padrť granitoids with selected intrusions of the CBPC. Data are from Holub et al. (1995, 1997b), René (1999), Sokol et al. (2000) and unpublished data of the authors.

Hornblende–biotite granodiorite is, based on the three studied samples, chemically homogeneous (63.2–64.3 wt. % SiO_2). It is characterized by relatively high contents of mafic elements (5.3–5.7 wt. % Fe_2O_{3tot}, 2.2–2.4 wt. % MgO) and low alkalis with a predominance of Na over K (3.1–3.4 wt. % Na_2O and 2.6–3.0 wt. % K_2O). Among trace elements, Rb reaches 102–127 ppm, Sr 207–232 ppm and Zr 120–139 ppm. Low contents of radioactive and ore elements (< 2–6 ppm U, 11–14 ppm Th, 7–8 ppm Nb and < 2 ppm Sn) indicate low degree of fractionation of this rock.

Biotite leucogranite sample is significantly more acid (74.7 wt. % SiO_2), poor in mafic components (1.55 wt. % Fe_2O_{3tot}, 0.44 wt. % MgO) and slightly enriched in potassium (4.94 wt. % K_2O). The contents of Rb and Sr are low (127 and 79 ppm, respectively) while U is slightly enriched (13 ppm).

4.2. Zircon U–Pb dating

Most of the studied zircons are clear to brownish and the morphological zircon populations present are equant to prismatic (stubby) grains, and euhedral needles. Using CL imaging (Fig. 5), internal zircon structures revealed common oscillatory zoning, typical of igneous zircon (e.g., Vavra 1990). Despite the morphological differences mentioned above, dominant feature of the studied zircons is recrystallization around the dark inclusions or cracks (often filled with SiO_2). In a few images, CL revealed sector zoning, characteristic of slowly grown zircons in plutonic environments (Hanchar and Miller 1993). The U–Pb measurements of 29 zircons yielded concordant ages between 337 Ma and 351 Ma, with a mean concordia age of 342.8 ± 1.1 Ma (2σ; Fig. 6; Electronic Supplement 3). The concordia zircon age is interpreted as the age of the crystallization of the Padrť Stock granodiorite.

4.3. Molybdenite Re–Os dating

The results of the Re–Os dating of molybdenite from Padrť are given in Tab. 2. The analyses of NIST 8599 molybdenite reference material yielded an age of 27.5 ± 0.2 Ma (2σ), which is well within given uncertainty of certified value (27.66 ± 0.1 Ma) and also similar to the ages of Porter and Selby (2010) and Lawley and Selby (2012). The studied molybdenite samples from Padrť (two independent molybdenite separations and analyses) have very high rhenium contents of 602 and 542 ppm as well as a high ^{187}Os contents of 2133 and 1934 ppb, yielding two Re–Os ages of 337.2 ± 2.4 and 339.8 ± 2.5 Ma.

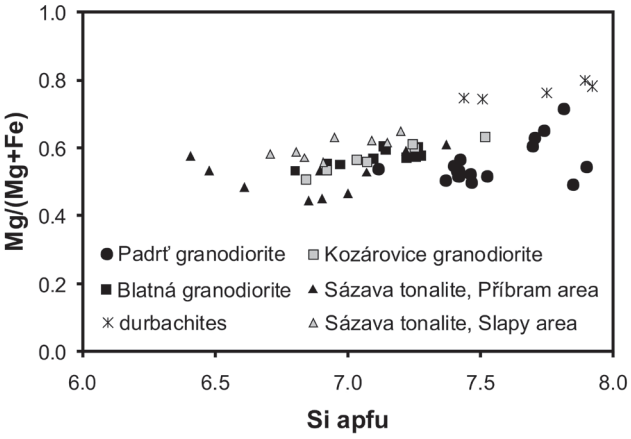

Fig. 3 Comparison of hornblende compositions from granitoids in the Padrť area and selected intrusions of the CBPC. Data from Poubová (1971, 1974), Poubová and Jurek (1976), Holub (1997), Sokol et al. (2000), Janoušek et al. (2000a), and unpublished data of the authors.

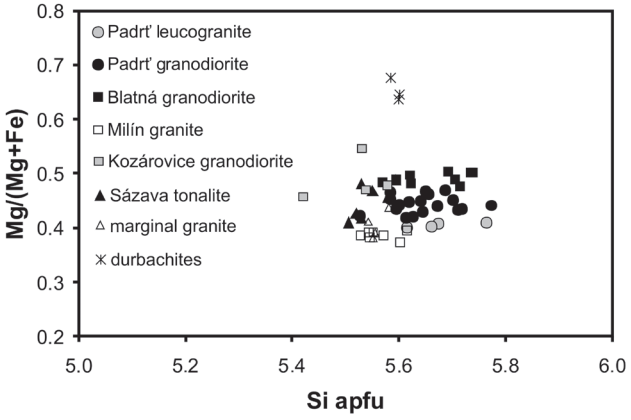

Fig. 4 Comparison of biotite compositions from Padrť and selected intrusions of the CBPC (data from Holub (1997), Sokol et al. (2000), Janoušek et al. (2000a) and unpublished data of the authors).

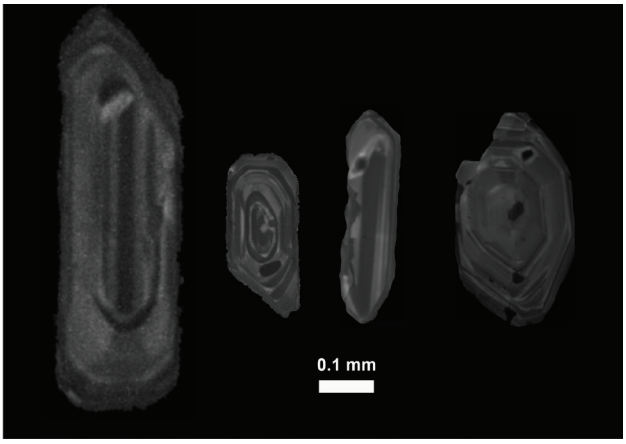

Fig. 5 Representative cathodoluminescence images of the dated zircon grains from the Padrť granodiorite (PAD-GR3).

Tab. 1 Whole-rock chemical compositions of granitoids (wt. %; trace elements in ppm)

	PAD-GR1	PAD-GR2	PAD-GR3	PAD-GR4
Locality	Teslíny Monastery	Teslíny Monastery	Přední Záběhlá	Kolvín
Latitude	49.63956	49.63931	49.65908	49.66535
Longitude	13.75028	13.75178	13.77606	13.73467
SiO_2	74.70	64.26	63.17	63.26
TiO_2	0.12	0.55	0.65	0.59
Al_2O_3	13.31	16.50	16.26	16.80
Fe_2O_3(tot.)	1.55	5.27	5.68	5.32
MgO	0.44	2.16	2.37	2.17
MnO	0.030	0.101	0.101	0.103
CaO	1.47	4.32	4.22	4.17
Li_2O	0.004	0.005	0.006	0.004
Na_2O	2.78	3.45	3.14	3.38
K_2O	4.94	2.64	2.98	2.81
P_2O_5	0.02	0.11	0.13	0.11
CO_2	< 0.01	0.02	0.01	< 0.01
S(tot.)	0.15	< 0.010	< 0.010	0.32
LOI	0.38	0.49	0.83	0.80
H_2O^-	0.09	0.07	0.14	0.12
S(equiv.)	–0.04	0.00	0.00	–0.08
Total	100.00	99.95	99.69	99.97
ASI	1.06	1.01	1.01	1.04
As	40	6	8	47
Cr	3	29	30	17
Cu	58	9	6	17
Mo	< 1	< 1	< 1	< 1
Nb	5	7	8	8
Ni	4	11	10	8
Pb	57	37	24	30
Rb	127	102	116	117
Sn	4	< 2	< 2	< 2
Sr	79	207	221	232
Th	26	14	11	12
U	13	< 2	2	6
Y	27	28	24	27
Zn	29	78	77	68
Zr	82	120	138	139

LOI – loss on ignition, S_{equiv} – correction reflecting the chemical bonding of part of the iron with sulfur instead with oxygen, ASI – alumina saturation index, defined as the molar ratio $Al_2O_3/(CaO+K_2O+Na_2O)$.

sive quartz, and (2) drusy vugs with euhedral quartz crystals. Quartz veins composed of massive quartz are up to 15 cm wide and represent the most common type in the studied area. Those with sparse vugs and euhedral crystals are much less frequent and usually less than 5 cm thick. Drusy vugs are related either to younger veins that crosscut the massive veins, or they locally develop in the core of massive veins.

Three generations of quartz were identified based on microscopic study: Q1 – the oldest, anhedral quartz grains, size of which may slightly increase from the vein rim towards the core. Individual grains are nearly opaque in their cores, mostly due to the presence of numerous smal and/or decrepitated fluid inclusions, and become more transparent near their rims. Notably Q1 quartz exhibits a moderate degree of ductile deformation and several phases of brittle deformation. The latter is recorded by numerous trails of secondary fluid inclusions, frequently occurring as parallel sets. Q2 – massive quartz (Q2a), it usually shows marked progressive grain-size gradation along the vein rim-to-core profile. Locally, in the core zone, vugs with subhedral quartz crystals (Q2b) are present. It is significantly less deformed than Q1. The amount of fluid inclusions in Q2 also decreases from grain core to grain rim. Q3 – forms sparse thin rims on the Q2 crystals. It differs from Q2, however, by having radial internal structure.

4.4. Fluid-inclusion study

4.4.1. Studied samples

Fluid inclusions were studied in six samples of quartz veins from the locality PAD-Q1 (Fig. 1b). Texturally they represent two principal types of quartz gangue: (1) mas-

4.4.2. Fluid inclusions

Two types of fluids were identified in the Q1 trough Q3, with respect to major components: aqueous–carbonic (H_2O–$CO_2 \pm CH_4$-salts) and aqueous-only (H_2O-salts).

Tab. 2 Re–Os data for the studied Padrť molybdenite and Henderson Mine reference material NIST 8599

Sample	Description	Re (ppm)	^{187}Os (ppb)	Age (Ma)
Os 296 (PAD-Q1/1)	Molybdenite sample PAD-Q1/1	602 (1)	2133 (13)	337.2 ± 2.4
Os 381 (PAD-Q1/2)	Molybdenite sample PAD-Q1/2	542 (2)	1934 (12)	339.8 ± 2.5
NIST 8599	Molybdenite reference material (Henderson Mine)	12.04 (3)	3.47 (3)	27.5 ± 0.2

Model Age was calculated assuming no presence of common Os. Total uncertainties shown are at 2-sigma level.

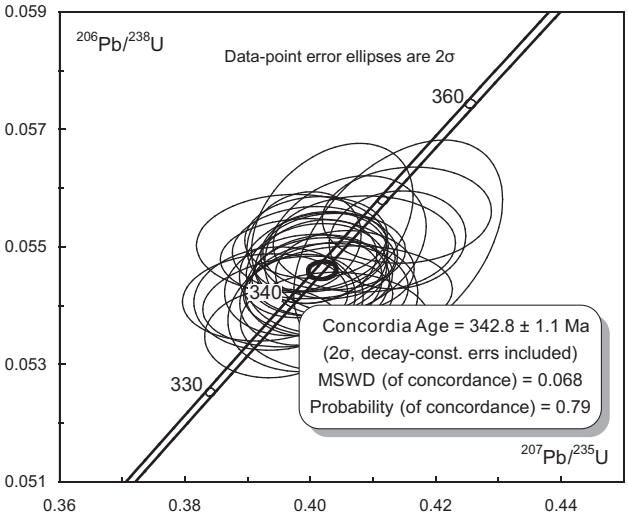

Fig. 6 U–Pb concordia diagram for zircons from the Padrť granodiorite (29 analyses). All data are plotted with 2σ uncertainties.

These form primary, pseudosecondary and secondary fluid inclusions (e.g., Roedder 1984). A relatively large number of totally or partially decrepitated fluid inclusions is observed in many of the studied samples. These are located not only in the anhedral and ductile/deformed Q1, but also in the undeformed and euhedral Q2. There seems to be a relation between the size, shape and composition of fluid inclusions and their ability to decrepitate naturally: the largest, mostly aqueous–carbonic and irregularly-shaped inclusions are frequently leaked.

4.4.3. Aqueous–carbonic inclusions (H_2O–CO_2 ± CH_4-salts)

The aqueous–carbonic fluid inclusions were identified mostly in the Q1 quartz, but also in older growth zones of Q2. They form both primary and secondary inclusions. Degree of fill is mostly homogeneous, reaching values 0.9 to 0.8. Temperatures of melting of solid CO_2 (Tm-CO_2) varied from –66.6 to –58.4 °C (with a subtle maximum from –61 to –59 °C) and together with melting of clathrate above 10 °C (from 10.6 to 13.8 °C), suggest low-salinity fluids (~ 2 wt. % eq. NaCl) and an admixture of CH_4 in the gaseous phase. Homogenization of the carbonic phase (Th-car) occurred from –20.0 to +27.7 °C (always to vapor; most data lie between 3 and 17 °C). In the absence of microRaman data we used the general relation between Th-car and Tm-CO_2 (van den Kerkhof and Thiéry 2001) in order to quantify the composition of the gaseous phase (10–30 mol. % CH_4, 90–70 mol. % CO_2; and 85–185 cm^3/mol). Final homogenization to the liquid phase occurred between 231 °C and 340 °C with a single maximum at 290–310 °C (Fig. 7). A few inclusions homogenized to vapor from 270 to 320 °C.

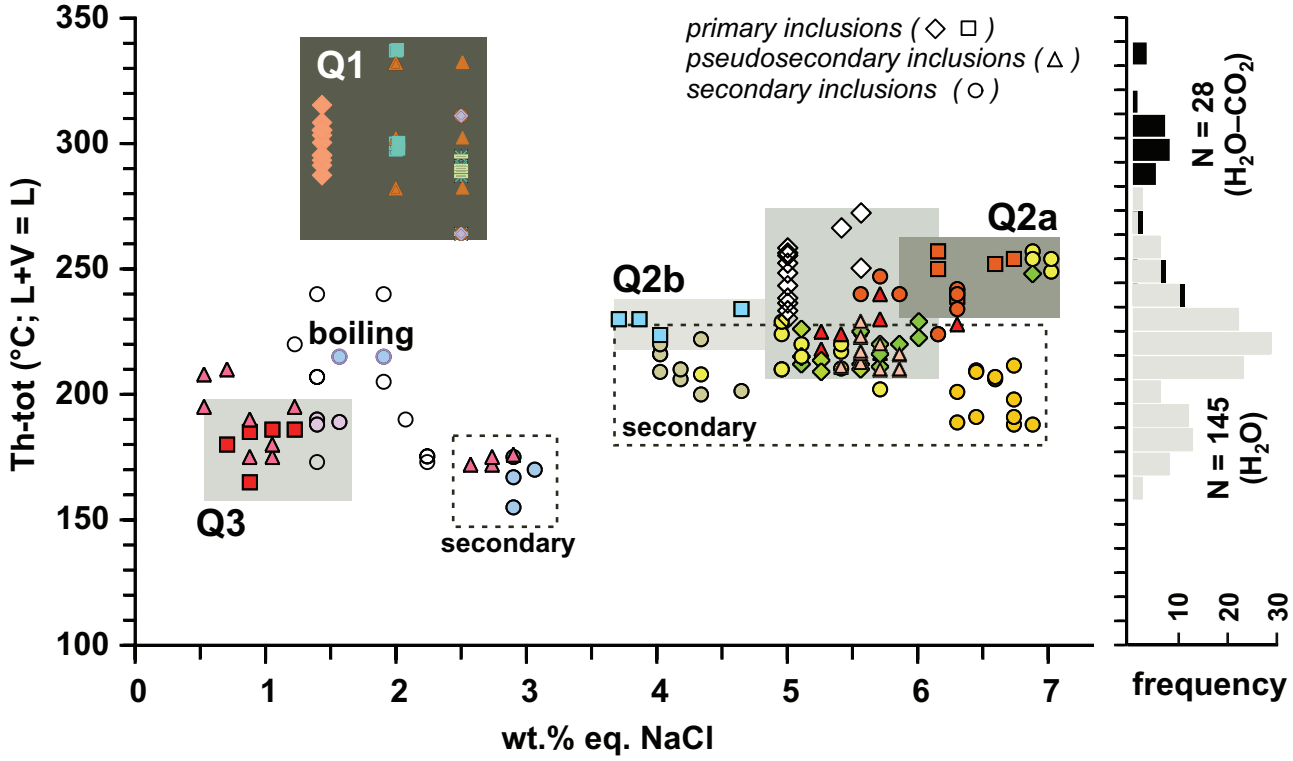

Fig. 7 Summary of measured microthermometric data for primary, pseudosecondary and secondary fluid inclusions. Corresponding fields of most representative data for Q1, Q2 and Q3 quartz are highlighted by shaded boxes. Summary histogram of final homogenization temperatures is plotted on the right side of the figure.

In addition to fluid-inclusion assemblages with homogeneous degree of fill, we noted also that of secondary fluid inclusions hosted by euhedral crystal (Q2b) that contained a mixture of monophase vapor (CO_2) inclusions, two-phase vapor- and liquid-rich inclusions and of rare monophase liquid (H_2O) inclusions. The following data were measured: Tm-CO_2 (–59.0 to –59.2 °C), Th-car (17.0 to 27.7 °C for two-phase inclusions and 3.6 °C for the monophase vapor inclusion; always to vapor state). Final homogenization of two-phase inclusions occurred from 230 to 280 °C; those representing end-members homogenized from 230 to 240 °C. We believe that this assemblage was trapped from an unmixed fluid and the measured 230–240 °C correspond therefore to the actual temperatures of Q2b formation.

4.4.4. Aqueous-only inclusions (H_2O-salts)

Q1 quartz All aqueous-only fluid inclusions in Q1 are clearly of secondary origin. They are related to trails (fractures) that crosscut more than two quartz grains and frequently are parallel with margins of the studied Q1 vein (pointing thus to their formation under approximately NE–SW oriented extension). They homogenize to liquid between 155 and 257 °C, with a marked maximum at 210 to 220 °C; salinity varies from 2.9 to 7.0 wt. % eq. NaCl.

Q2 quartz At least three generations of aqueous-only fluids can be identified in Q2: the oldest one is represented by three-dimensional clusters of primary liquid-rich fluid inclusions in the "dark" cores of anhedral quartz grains. They display mostly homogeneous degree of fill (0.9). They gradually pass into the next inclusion generation that is hosted by transparent outer rims/zones of Q2. Inclusions here are similar to those from cores, except for slightly lower degree of fill (0.85–0.80) and increasing abundance of vapor-rich and vapor-only fluid inclusions (both types indicate that boiling of fluid locally occurred). Third (and fourth) generation of inclusions is represented by well-defined secondary trails, some of which contain a heterogeneous mixture of boiled fluids (highly variable degree of fill).

Inclusions representing the early fluids characterize broadly variable homogenization temperatures of 160–226 °C (to liquid) and a narrow range of salinities (5.0 to 5.9 wt. % eq. NaCl). Primary inclusions of the next generation (grain rims) show slightly higher homogenization temperatures (223.7 to 234 °C; to liquid), but more variable and generally lower salinities (1.9 to 4.6 wt. % eq. NaCl). Pseudosecondary inclusions from the same zone yielded even lower temperatures (172 to 210 °C; to liquid) and salinities (0.7–2.9 wt. % eq. NaCl) and the same holds for clearly secondary inclusions (188–190 °C, 0.5–1.6 wt. % eq. NaCl). A few vapor-rich secondary fluid inclusions homogenized to vapor at *c.* 200–215 °C. Conditions of late boiling can bet thus set at about 200 °C.

Q3 quartz Sparse, likely primary fluid inclusions homogenized from 165 to 186 °C (to liquid); salinity is estimated to be 0.9–1.2 wt. % eq. NaCl.

5. Discussion

5.1. Comparison of the Padrť Stock with granitoids of the CBPC

Granitoids of the CBPC are classified into several major suites: normal calc-alkaline Sázava suite (e.g., gabbros, Sázava tonalite, Marginal granite), high-K calc-alkaline Blatná suite (e.g., Blatná granodiorite, Kozárovice granodiorite, Červená granodiorite, Milín granite), K- and Mg-rich Čertovo Břemeno suite (e.g., Sedlčany granite, durbachites), and peraluminous Maršovice suite (e.g., Kozlovice and Maršovice granodiorites) (Janoušek et al. 1995; Holub et al. 1997b; Janoušek and Skála 2011 and references therein). Published geological maps and papers (Čepek and Zoubek eds. 1961; Holub et al. 1997b; Mašek ed. 1990) assigned the granitoids from Padrť to the types later included into Sázava or the Blatná suites. However, all mentioned authors classified the granitoids probably only on the basis of macroscopic and microscopic observations; whole-rock chemical data were not available, except for an average of two analyses in an unpublished report by Vlašímský (1976).

But even on the basis of our new chemical analyses of rocks and minerals, the Padrť granitoids cannot be classified unequivocally. Figure 2 compares the Padrť granitoids with selected granitoid types of the CBPC with similar SiO_2 contents: the Sázava tonalite, Blatná granodiorite, Červená granodiorite, Milín granite, and the Marginal granite. The contents of MgO, CaO and K_2O in Padrť granodiorite vary between values typical of the Sázava and Blatná suites (Fig. 2). In addition, K_2O vs. Rb and Rb vs. Sr diagrams further highlight the intermediate nature of the Padrť granodiorite between the typical compositions of the Sázava and Blatná suites. The chemical composition of the Teslíny leucogranite is close to the Marginal granite according to Holub et al. (1997b) and granites from the area of Underground Gas Storage Facility near Příbram (Sokol et al. 2000). Two samples from the Padrť Stock analyzed by Vlašímský (1976) were of a more basic composition (SiO_2 ~ 57.7 wt. %) but their exact location in the field is unknown.

Regarding the amphibole composition, analyses from Padrť are richer in silica than early magmatic hornblende from the Sázava and Blatná intrusions (mostly in the range 7.4–7.9 apfu Si, Fig. 3). Such composition is typi-

cal of the magmatic amphibole from durbachites (e.g., Holub 1997) or late amphiboles from the Sázava tonalite (Poubová and Jurek 1976) and Kozárovice granodiorite (Janoušek et al. 2000a). Biotite from Padrť granodiorite fills the gap between compositions of biotite from typical Blatná granodiorite and Milín granite, containing somewhat more Si than biotites from the Sázava suite in the Příbram area (Sokol et al. 2000) (Fig. 4).

The data suggest the succession of two intrusions in the Teslíny area: (i) hornblende–biotite Padrť granodiorite cropping out between Teslíny and Přední Zaběhlá, with a small isolated apophysis at Kolvín, and (ii) Teslíny leucogranite forming a mostly hidden body between Teslíny (including two drilling sites described by Fediuk 2008) and the southern end of the Upper Padrť Pond.

The Teslíny leucogranite intrusion includes tourmaline- and locally also garnet-bearing pegmatite-like rock described by Ambrož (1865), and again briefly by Fediuk (2008), which we found as blocks between Teslíny and the southern Padrť Pond. The relationship between leucogranite and granodiorite cannot be resolved. The leucogranite is most similar to the Marginal granite (*sensu* Janoušek and Skála 2011), whereas correlation between the hornblende–biotite granodiorite and the other intrusions remains unclear.

5.2. Geochronology

Morphology, internal zoning, and Th/U ratios can be used in the interpretation of zircon origins (Pupin 1980; Hoskin and Schaltegger 2003). Constant Th/U ratios through time are interpreted to reflect closed-system behavior, whereas higher Th/U in overgrowths can indicate the occurrence of Th-rich inclusions (monazite, allanite etc.; Harley et al. 2007). All Padrť zircons show Th/U values below 0.5 (*c.* 50–160 ppm Th, 120–450 ppm U; see Electronic Supplement 3), and the majority of them yield a mean value at 0.3. This uniform, intermediate Th/U ratio suggests an origin from a single magmatic source and it appears that the Th/U is more variable than proposed by Hoskin and Schaltegger (2003). The average Th/U ratios of Padrť magmatic zircons are somewhat lower than those of oscillatory zoned zircon grains from Blatná and Kozárovice granodiorites (Janoušek et al. 2010).

The U–Pb zircon age of the studied Padrť granodiorite of 342.8 ± 1.1 Ma is in the range obtained for younger types of the CBPC by U–Pb or Pb–Pb zircon dating. In spite of the chemical contrasts between intrusions within the CBPC (see Holub et al. 1997b; Janoušek et al. 1995, 2000b), the age span of main-phase plutons is relatively restricted within *c.* 15–20 My, between 354 ± 4 and 337 ± 1 Ma. Individual published ages are as follows (all errors are 2σ): (i) calc-alkaline rocks of the *Sázava suite*, 354 ± 4 Ma (Janoušek et al. 2004) and 346 ± 10 Ma (Holub et al 1997a); (ii) high-K calc-alkaline rocks, *Blatná and Kozárovice granodiorites*, 347 ± 2 Ma and 346 ± 2 Ma, (Janoušek et al. 2010), *Klatovy granodiorite*, 347 $^{+4}/_{-3}$ Ma (Dörr and Zulauf 2010); *Nýrsko granite*, 339 ± 2 Ma (Dörr and Zulauf 2010). The youngest ages within the CBPC were obtained for (iii) potassic to ultrapotassic rocks, *Čertovo břemeno durbachite* (343 ± 6 Ma; Holub et al. 1997a) and *Tábor quartz syenite* (337 ± 1 Ma; Janoušek and Gerdes 2003).

The granodiorite–tonalite intrusive bodies of the Štěnovice and Čistá plutons, located within the TBU, are significantly older than granitoids of the CBPC. These plutons were dated using zircon U–Pb laser ablation ICP-MS (Žák J et al. 2010) and the Pb–Pb evaporation technique (Venera et al. 2000), which yielded mutually comparable ages (375 ± 2 Ma and 373 ± 1 Ma, respectively).

Zircon U–Pb ages for the Bohutín Stock are lacking. There are some old K–Ar ages which were clearly influenced by excess argon and thus yielded unrealistically high Silurian ages (e.g., Vlašímský 1982). Žák K et al. (1998) dated hornblende from the Bohutín Stock by the Ar–Ar method. The argon released during the low-temperature steps indicated older ages up to 370 Ma, while the plateau age (argon released at 1150–1600 °C) was 348.5 ± 0.5 Ma (Žák K et al. 1998). Nevertheless, it was clear that this plateau age was also affected by excess argon, which was probably inherited when this narrow intrusive stock intruded Neoproterozoic rocks. When we use only the data from the 9 highest temperature steps (1275–1600 °C), the calculated isochron age is 342 ± 0.3 Ma, which is similar to the zircon U–Pb age of the Padrť Stock. It is therefore possible that intrusion of Bohutín and Padrť magmas could have been roughly coeval. However, zircon ages from the Bohutín Stock are needed.

The newly obtained Re–Os ages of molybdenite mineralization spatially related to the Padrť Stock (337.2 ± 2.4 and 339.8 ± 2.5 Ma) are somewhat younger than the Re–Os age of molybdenite from the Petráčkova hora gold deposit in the Rožmitál Block (344.4 ± 2.8 Ma; Zachariáš et al. 2001). The Rožmitál Block is surrounded mostly by granitoids belonging to the Blatná suite (347 ± 2 Ma; Janoušek et al. 2010). For small porphyritic granitoid bodies located within the Rožmitál Block, rather controversial age results of *c.* 343–355 Ma have been obtained (see review in Zachariáš et al. 2001). In case of the Padrť Stock, the zircon age on the one hand, and the two molybdenite ages on the other, are within the error different. Therefore, estimating the temperature of molybdenite formation is crucial for the explanation of this possible age gap (see below in Section 5.3).

Detailed study of the age relationships between small intrusive stocks and related mineralization can

improve our understanding of the chronology of individual pulses of hydrothermal vein mineralizations in the Příbram Ore Region. Cross-cutting relations show that both quartz veins with molybdenite and quartz veins with gold postdated the intrusion of the Bohutín Stock (Píša 1966; Bambas 1990). The Bohutín intrusive body and the quartz–molybdenite as well as quartz–gold veins were later cross-cut by the younger Ag–Pb–Zn ± Sb veins (Píša 1966). Similar types of mineralizations occur around the Padrť Stock – molybdenite and antimonite occurrences (Ambrož 1865). Indications of Pb–Zn and Au mineralizations were found by regional ore prospection (Píša et al. 1976; Studničná 1989). The largest difference with respect to hydrothermal ore mineralizations can be viewed in the abundance of arsenopyrite in the surroundings of the Padrť Stock, which is uncommon in the Bohutín area.

Were the molybdenite mineralization at Padrť and Bohutín contemporaneous, the obtained molybdenite ages define the older age limit for the Ag–Pb–Zn ± Sb veins. Field evidence, and evaluation of stable isotope data, fluid types and temperatures of deposition show that the Ag–Pb–Zn ± Sb veins were older than the U mineralization of the Příbram Ore Region (e.g., Vlašímský et al. 1995; Žák K and Dobeš 1991; Škácha et al. 2009). The U mineralization of the main uranium ore district in the southern part of the Příbram Ore Region was repeatedly dated by the U–Pb method on uraninite. Probably the most concordant and reliable age data of 275 ± 4 to 278 ± 4 Ma have been obtained by Anderson (1987), which set the younger age limit for the Ag–Pb–Zn ± Sb veins. Škácha et al. (2009) attempted to date uraninite postdating the Ag–Pb–Zn veins directly at the Příbram – Březové Hory deposit in the polymetallic part of the Příbram Ore Region. The uraninite contained high levels of common lead and the mathematical regression of the data gave only a rough age estimate of 269.8 ± 20.3 Ma. Chemical (electron-microprobe) dating using the only uraninite grain without galena inclusions (supposing no common lead in uraninite) yielded an age of 263.2 ± 8.9 Ma. These data probably indicate that the U mineralizations in both parts of the Příbram Ore Region could have been roughly synchronous. The large interval between the magmatic processes and formation of U mineralization was probably related to the time necessary for erosion of the overlying rocks, opening of brittle faults, and activation of the circulation of shallow-crustal fluids, as evidenced by fluid-inclusion and stable-isotope studies (Žák K and Dobeš 1991).

The formation of economically and historically important Ag–Pb–Zn ± Sb mineralization (production of 3.500 t Ag, 480.000 t Pb, 260.000 t Zn; Bambas 1990) is therefore still chronologically poorly constrained within an age interval of *c.* 60 My (337 to *c.* 275 Ma). With respect to the presence of Sn and W minerals in the deep part of the Březové Hory deposit (Bambas 1990), and relatively high temperatures of deposition inferred from fluid inclusions (Žák K and Dobeš 1991), the formation of the Ag–Pb–Zn ± Sb veins was probably closer to 337 than to 275 Ma.

5.3. Conditions of quartz and molybdenite formation at Padrť

Optical microscopy and fluid-inclusion microthermometry revealed the presence of at least three generations of quartz gangue at Padrť, at the locality with occurrence of molybdenite. Early quartz (Q1) corresponds to formation of the most common quartz veins dominated by massive "saccharoidal" quartz gangue. It precipitated from aqueous carbonic fluids that were relatively rich in CH_4 (10–30 mol. % in gaseous phase), were of low-salinity (*c.* 2 wt. eq. NaCl) and had homogenization temperatures clustered around 300 °C.

Younger quartz (Q2), that forms euhedral crystals in the vugs in the Q1, or its own late veins, exhibits higher salinities (6–7 wt. % eq. NaCl) and lower homogenization temperatures (230–260 °C; Fig. 8). The Q2 gradually evolved through the time to slightly lower salinities (4–5 wt. % eq. NaCl) and temperatures (*c.* 190–220 °C).

Significantly lower salinity (*c.* 1 wt. % eq. NaCl) of fluids associated with the Q3 indicate their late hydrothermal origin, most probably unrelated to the formation of Q1 and Q2. It differs from Q2 by having radial internal structure, that might indicate its precipitation from silica-saturated solutions and/or original presence of chalcedony that later recrystallized with time to α-quartz.

It is uncertain whether the Q1 and Q2 represented two genetically and chronologically unrelated events, or whether they were the products of a single, more or less, continuous process. Apparent optical transition of Q1 into Q2 in some samples, as well as existence of both aqueous–carbonic and aqueous-only fluids in the older growth zones of Q2 seem to support the later hypothesis. This is further supported by similar slopes of fluid isochores for both aqueous–carbonic and aqueous-only fluids (Fig. 8). An argument that supports the former hypothesis is, however, the difference in fluid salinities.

Likely P–T conditions of the Q1, Q2, and Q3 formation are summarized in Fig 8. As already mentioned above, the final stages of Q2 evolution are well-constrained by the heterogeneous fluid assemblage unmixed at *c.* 230–240 °C and *c.* 60 MPa. This corresponds to a depth of about 2.2 km, if a fully lithostatic regime is considered. Formation of Q1 is restricted to a P–T range delimited by steep isochores of aqueous–carbonic fluids; they approach the solidus of water-saturated granite melt

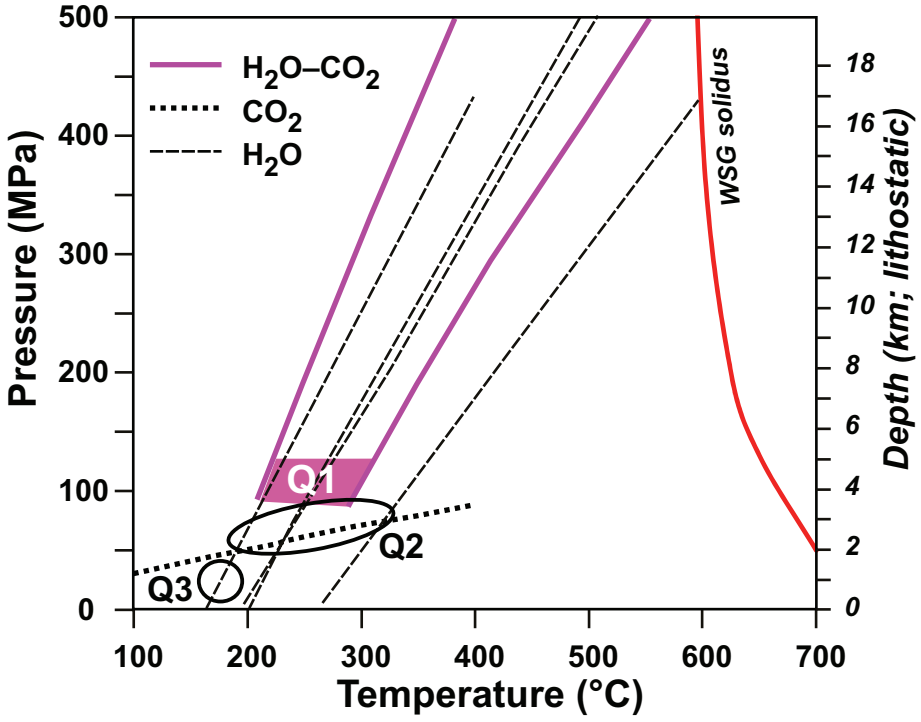

Fig. 8 Representative isochores for aqueous–carbonic (thick solid lines), aqueous-only (thin dashed lines) and for the monophase carbonic–gaseous (thick dotted line) inclusions. Likely conditions of Q2 and Q3 formation are shown by ellipses, those for Q1 are highlighted by shading. The line labelled 'WSG' is estimated water-saturated granite melt solidus.

at > 500 MPa, i.e. at a depth greater than 15 km. This is, in light of the practically unmetamorphosed character of the Neoproterozoic and Cambrian sediments (except in contact zone of the stock) an unrealistically great depth. Therefore we may conclude that fluids precipitating Q1 did not exsolve from the Padrť granodiorite melt, despite the fact that they are spatially closely related. This also explains well the age difference between the magmatism and molybdenite mineralization. We consider 5 km (130 MPa) as a reasonable estimate of maximum depth of the Padrť Stock emplacement. Thus, we may conclude that Q1 formed at temperature not higher than *c.* 320 °C. Formation of molybdenite, that is younger than most of Q1, but older than Q2b, can therefore be estimated at 280–300 °C. Finally, the widespread presence of decrepitated aqueous–carbonic inclusions in the Q1 may have resulted from thermal and pressure stresses associated with the intrusion of the Padrť Stock. In this case, Q1 quartz veins would be even older than the Padrť intrusion.

The present study, and earlier conclusions of Vlašímský (1982) and Žák K and Dobeš (1991), show that with respect to regional position, time span, fluid types and mineralization conditions, the source of the economically most important Ag–Pb–Zn ± Sb hydrothermal vein deposits could not have been fluids derived during crystallization of CBPC granitoids and satellite stocks. The source of fluid components of this mineralization type had to be in a deeper crust, probably related to clastic metasedimentary rocks (see Beaudoin et al. 1999).

6. Conclusions

The present geochemical and geochronological study leads to the following conclusions:

1. At least two types of granitoids crop out in the Padrť area, fine- to medium-grained hornblende–biotite Padrť granodiorite, and fine- to medium-grained partly porphyritic biotite Teslíny leucogranite accompanied by pegmatoid rock with tourmaline ± garnet.
2. The whole-rock contents of MgO, CaO and K_2O in the Padrť granodiorite vary between values typical of the Sázava and Blatná suites of the CBPC. Furthermore, variations in K_2O, Rb and Sr highlight the intermediate compositions of the Padrť granodiorite between the typical values of the Sázava and Blatná suites. In contrast, chemical composition of the Teslíny leucogranite is close to the Marginal granite (probably part of the Sázava suite) of the CBPC. Amphibole compositions from Padrť differ from early magmatic amphiboles of both the Sázava and Blatná suites. The studied amphiboles are more siliceous (often actinolitic), which is otherwise more typical of the Čertovo bremeno suite of the CBPC or some late amphiboles in the Sázava and Blatná suites. Biotite compositions from Padrť fill the gap between those from typical Blatná granodiorite and Milín granite of the CBPC.
3. Oscillatory-zoned zircons from the Padrť granodiorite yielded a concordant age of 342.8 ± 1.1 Ma (2σ), which is interpreted as the intrusive age.
4. Two Re–Os datings of molybdenite from quartz veins within a quartzite lens in close exo-contact of the

Padrť granodiorite yielded ages of 337.2 ± 2.4 and 339.8 ± 2.5 Ma.

5. Several generations of quartz were identified in the quartz veins. The molybdenite mineralization was younger than Q1, but older than Q2b quartz. Quartz fluid-inclusion data indicate deposition of molybdenite at 280–300 °C at depths between 2.2 and 5 km below the original surface.

Acknowledgements. This study is a part of research focused on further development of Re–Os dating of sulfidic minerals financed by the Czech Science Foundation (GAČR) project No. GA13-15390S, and by RVO67985831 institutional support. The permission to perform the field work and sampling inside the Brdy Military Training Area issued by the Military Training Area Office to K. Žák was greatly appreciated. Comments and corrections by reviewers F.V. Holub and K. Johnson, and by the journal editors J. Žák and V. Janoušek, significantly improved the manuscript. Our research team was struck by the loss of Jiří Litochleb, who passed away on February 26, 2014.

Electronic supplementary material. Supplementary data for this paper, including hornblende and biotite mineral analyses as well as results of zircon U–Pb dating by the LA ICP-MS method, are available online at the Journal web site (*http://dx.doi.org/10.3190/jgeosci.177*).

References

Ambrož F (1865) Geologische Studien aus der Gegend von Padrť. Jb K-Kön geol Reichsanst 15: 215–228

Anderson EB (1987) Izotopno-geokhronologicheskoe issledovanie uranovych mestorodzhenii CHSSR (Isotopic-geochronological investigation of the uranium ore deposits of Czechoslovakia). Unpublished Report 1862-87, Czechoslovak Uranium Industry, Příbram, pp 1–67 (in Russian)

Bakker RJ (1997) CLATHRATES: computer programs to calculate fluid inclusion V–X properties using clathrate melting temperatures. Comp Geosci 23: 1–18

Bakker RJ (1999) Adaptation of the Bowers and Helgeson (1983) equation of state to the H_2O–CO_2–CH_4–N_2–NaCl system. Chem Geol 154: 225–236

Bakker RJ (2003) Package FLUIDS 1. Computer programs for analysis of fluid inclusion data and for modelling bulk fluid properties. Chem Geol 194: 3–23

Bambas J (1990) Březohorský rudní revír (Březové Hory ore district). Symposium Hornická Příbram ve Vědě a Technice, Příbram, pp 1–204 (in Czech)

Beaudoin G, Leach DL, Hofstra A, Seifert T, Žák K (1999) Silver–lead–zinc veins: a descriptive model. In: Stanley CJ et al. (eds) Mineral Deposits: Processes to Processing, Vol 2. Balkema, Rotterdam, pp 923–926

Bodnar RJ (1993) Revised equation and table for determining the freezing point depression of H_2O–NaCl solutions. Geochim Cosmochim Acta 57: 683–684.

Creaser RA, Papanastassiou DA, Wasserburg GJ (1991) Negative thermal ion mass spectrometry of osmium, rhenium, and iridium. Geochim Cosmochim Acta 55: 397–401

Čepek L, Zoubek V (eds) (1961) Geologická mapa ČSSR 1:200 000, list M-33-XX Plzeň (Geological map of Czechoslovakia 1:200 000, sheet M-33-XX Plzeň). Czech Geological Survey, Prague (in Czech)

Dempírová L (2010) Evaluation of SiO_2, Na_2O, MgO, K_2O determinations in silicate samples by *z*-score obtained from nineteen interlaboratory tests. Zpr geol výzk v r 2009: 323–326 (in Czech)

Dempírová L, Šikl J, Kašičková R, Zoulková V, Kříbek B (2010) The evaluation of precision and relative error of the main components of silicate analyses in Central Laboratory of the Czech Geological Survey. Zpr geol výzk v r 2009: 326–330 (in Czech)

Dörr W, Zulauf G (2010) Elevator tectonics and orogenic collapse of a Tibetan-style plateau in the European Variscides: the role of the Bohemian shear zone. Int J Earth Sci 99: 299–325

Dudek A, Fediuk F (1956) Bohutínský křemenný diorit (Bohutín quartz diorite). Acta Univ Carol, Geol 2: 149–169 (in Czech)

Fediuk F (2008) Granitoids and metamorphosed Proterozoic in the Padrť-ponds area, SW Brdy-Highland. Zpr geol výzk v r 2007: 21–22 (in Czech)

Hajná J, Žák J, Kachlík V (2011) Structure and stratigraphy of the Teplá–Barrandian Neoproterozoic, Bohemian Massif: a new plate-tectonic reinterpretation. Gondwana Res 19: 495–508

Hanchar JM, Miller CF (1993) Zircon zonation patterns as revealed by cathodoluminescence and backscattered electron images: implications for interpretation of complex crustal histories. Chem Geol 110: 1–13

Harley SL, Kelly NM, Möller A (2007) Zircon behaviour and the thermal histories of mountain chains. Elements 3: 25–30

Holub FV, Janoušek V, Košler J (1995) European network of Laboratories, Granites – Guide Book to Field meeting in the Bohemian Massif, Czech Republic, October 4–9, 1995, Prague, pp 1–83

Holub FV (1997) Ultrapotassic plutonic rocks of the durbachite series in the Bohemian Massif: petrology, geochemistry and petrogenetic interpretation. Sbor geol Věd, Ložisk Geol Mineral 31: 5–25

Holub FV, Cocherie A, Rossi P (1997a) Radiometric dating of granitic rocks from the Central Bohemian Plutonic Complex: constraints on the chronology of thermal and tectonic events along the Barrandian–Moldanubian boundary. C R Acad Sci Paris, Sciences de la Terre et des planétes 325: 19–26

Holub FV, Machart J, Manová M (1997b) The Central Bohemian Plutonic Complex: geology, chemical compo-

sition and genetic interpretation. Sbor geol Věd, Ložisk Geol Mineral 31: 27–50

Hoskin PWO, Schaltegger U (2003) The composition of zircon and igneous and metamorphic petrogenesis. In: Hanchar JM, Hoskin PWO (eds) Zircon. Mineralogical Society of America and Geochemical Society Reviews in Mineralogy and Geochemistry 53: 27–62

Jackson SE, Pearson NJ, Griffin WL, Belousova EA (2004) The application of laser ablation-inductively coupled plasma-mass spectrometry to in situ U–Pb zircon geochronology. Chem Geol 211: 47–69

Janoušek V, Gerdes A (2003) Timing the magmatic activity within the Central Bohemian Pluton, Czech Republic: conventional U–Pb ages for the Sázava and Tábor intrusions and their geotectonic significance. J Czech Geol Soc 48:70–71

Janoušek V, Skála R, eds (2011) Bohemian Geological Enigmas: Variscan High-pressure Granulites, Ultrapotassic magmatites and Tektites. Goldschmidt 2011 Post-Conference Field Trip, August 20–22, 2011, Excursion Guide, Prague, pp 3–38

Janoušek V, Rogers G, Bowes DR (1995) Sr–Nd isotopic constraints on the petrogenesis of the Central Bohemian Pluton, Czech Republic. Geol Rundsch 84: 520–534

Janoušek V, Bowes DR, Braithwaite CJR, Rogers G (2000a) Microstructural and mineralogical evidence for limited involvement of magma mixing in the petrogenesis of a Hercynian high-K calc-alkaline intrusion: the Kozárovice granodiorite, Central Bohemian Pluton, Czech Republic. Trans Roy Soc Edinb, Earth Sci 91:15-26

Janoušek V, Bowes DR, Rogers G, Farrow CM, Jelínek E (2000b) Modelling diverse processes in the petrogenesis of a composite batholith: the Central Bohemian Pluton, Central European Hercynides. J Petrol 41: 511–543

Janoušek V, Braithwaite CJR, Bowes DR, Gerdes A (2004) Magma-mixing in the genesis of Hercynian calc-alkaline granitoids: an integrated petrographic and geochemical study of the Sázava intrusion, Central Bohemian Pluton, Czech Republic. Lithos 78: 67–99

Janoušek V, Wiegand BA, Žák J (2010) Dating the onset of Variscan crustal exhumation in the core of the Bohemian Massif: new U–Pb single zircon ages from the high-K calc-alkaline granodiorites of the Blatná suite, Central Bohemian Plutonic Complex. J Geol Soc, London 167: 347–360

Knížek M (2013) Radiální tektonika Barrandienu (Radial tectonics of the Barrandian area). Unpublished PhD Thesis, Masaryk University, Brno, pp 1–59 (in Czech)

Kohút M, Trubač J, Novotný L, Ackerman L, Demko R, Bartalský B, Erban V (2013) Geology and Re–Os molybdenite geochronology of the Kurišková U–Mo deposit (Western Carpathians, Slovakia). J Geosci 58: 271–282

Lawley CJM, Selby D (2012) Re–Os geochronology of quartz-enclosed ultrafine molybdenite: implications for ore geochronology. Econ Geol 107: 1499–1505

Li J, Liang X-R, Xu J-F, Suzuki K, Dong Y-H (2010) Simplified technique for the measurements of Re–Os isotope by multicollector inductively coupled plasma mass spectrometry (MC-ICP-MS). Geochem J 44:73–80

Ludwig KR (2003) User's manual for ISOPLOT 3.0, A Geochronological Toolkit for Microsoft Excel. Berkeley Geochronology Center Special Publications 4: pp 1–70

Markey R, Stein HJ, Hannah JL, Morgan JW, Zimmerman A, Selby D, Creaser RA (2007) Standardizing Re–Os geochronology: a new molybdenite reference material (Henderson, USA) and the stoichiometry of Os salts. Chem Geol 244: 74–87

Mašek J ed (1990) Geologická mapa České republiky 1 : 50 000, 22-12 Březnice (Geological map of the Czech Republic 1 : 50 000, sheet 22-12 Březnice). Czech Geological Survey, Prague (in Czech)

Merlet C (1994) An accurate computer correction program for quantitative electron-probe microanalysis. Microchim Acta 114: 363–376

Paton C, Woodhead JD, Hellstrom JC, Hergt JM, Greig A, Maas R (2010) Improved laser ablation U–Pb zircon geochronology through robust downhole fractionation correction. Geochem Geophys Geosys 11: Q0AA06, doi: 10.1029/2009gc002618

Paton C, Hellstrom J, Paul B, Woodhead J, Hergt J (2011) Iolite: freeware for the visualisation and processing of mass spectrometric data. J Anal Atom Spec 26: 2508–2518

Píša M (1966) Minerogenesis of the Pb–Zn deposit at Bohutín near Příbram. Sbor geol Věd, Ložisk Geol 7: 5–164

Píša M et al. (1976) Geologie a metalogeneze příbramské rudní oblasti (Geology and metallogeny of the Příbram ore region). Unpublished report P025943, Geofond, Prague (in Czech)

Porter SJ, Selby D (2010) Rhenium–Osmium (Re–Os) molybdenite systematics and geochronology of the Cruachan granite skarn mineralization, Etive Complex: implications for emplacement chronology. Scot J Geol 46: 17–21

Poubová M (1971) Optical and chemical characteristics of some hornblendes from the Central Bohemian Pluton. Krystalinikum 7: 119–133

Poubová M (1974) Composition of amphiboles and rock type subdivisions in the Central Bohemian Pluton. Krystalinikum 10: 149–179

Poubová M, Jurek K (1976) Recrystalization of hornblende into actinolite in the dioritic rocks, Central Bohemian Pluton. Věst Ústř Úst geol 51: 331–337

Pupin JP (1980) Zircon and granite petrology. Contrib Mineral Petrol 73: 207–220

René M (1999) Petrogenesis of granitoids in the Červená type (Central Bohemian Pluton). Acta Montana, Series A 14: 81–97

Roedder E (ed) (1984) Fluid Inclusions. Mineralogical Society of America Reviews in Mineralogy 12: 1–646

Schoenberg R, Nägler TF, Kramers JD (2000) Precise Os isotope ratio and Re–Os isotope dilution measurements down to the picogram level using multicollector inductively coupled plasma mass spectrometry. Int J Mass Spectrom 197: 85–94

Selby D, Creaser RA (2001) Re–Os geochronology and systematics in molybdenite from the Endako porphyry molybdenium deposit, British Columbia, Canada. Econ Geol 96: 197–204

Slavík F (1915) Chiastolitické břidlice v okolí rožmitálském (Chiastolithic shales in surroundings of Rožmitál). Rozpr Čes Akad Vědy Slovesn Umění, Tř II 24: 1–15 (in Czech)

Smoliar MI, Walker RJ, Morgan JW (1996) Re–Os ages of group IIA, IIIA, IVA, and IVB iron meteorites. Science 271: 1099–1102

Sokol A, Domečka K, Breiter K, Janoušek V (2000) Underground gas storage near Příbram – a source of new information about granitoids of the Central Bohemian Pluton. Věst Čes geol úst 75: 89–104

Studničná B (1989) Nové poznatky ložiskového průzkumu v oblasti rožmitálské tektonické kry (New data from ore-deposit prospection in the Rožmitál tectonic block). Studie z Dějin Hornictví III. Hornická Příbram ve vědě a technice, Příbram, pp 1–22 (in Czech)

Škácha P, Goliáš V, Sejkora J, Plášil J, Strnad L, Škoda R, Ježek J (2009) Hydrothermal uranium–base metal mineralization of the Jánská vein, Březové Hory, Příbram, Czech Republic: lead isotopes and chemical dating of uraninite. J Geosci 54: 1–13

Van den Kerkhof AM, Thiéry R (2001) Carbonic inclusions. Lithos 55: 27–47

Vavra G (1990) On the kinematics of zircon growth and its petrogenetic significance: a cathodoluminescence study. Contrib Mineral Petrol 106: 90–99

Venera Z, Schulmann K, Kröner A (2000) Intrusion within a transtensional tectonic domain: the Čistá granodiorite (Bohemian Massif) – structure and rheological modelling. J Struct Geol 22: 1437–1454

Vlašímský P (1976) Petrogeneze a geochemie sedimentů a magmatitů Příbramské rudní oblasti (Petrogenesis and geochemistry of sedimentary and magmatic rocks of the Příbram ore region). Unpublished report P26132, Geofond, Prague (in Czech)

Vlašímský P (1982) The Příbram ore district; rock geochemistry and potential sources of hydrothermal mineralization. J Geol Sci, Econ Geol Mineral 24: 49–99

Vlašímský P, Žák K, Komínek J, Patočka F (1995) Late Variscan hydrothermal uraninite–anthraxolite deposits of the Příbram ore region, Bohemian Massif: geology and genetic features of the largest uranium vein-type deposits of the Czech Republic. In: Pašava J, Kříbek B, Žák K (eds) Mineral Deposits: From Their Origin to Their Environmental Impacts. Proceedings of Third Biennial SGA Meeting, Prague, August 28–31, 1995. Balkema, Rotterdam, pp 397–400

Völkening J, Walczyk T, Heumann KG (1991) Osmium isotope ratio determinations by negative thermal ionization mass spectrometry. Int J Mass Spectrom Ion Process 105: 147–159

Walczyk T, Heumann KG (1993) Iridium isotope ratio measurements by negative thermal ionization mass-spectrometry and atomic-weight of iridium. Int J Mass Spectrom Ion Process 123: 139–147

Wiedenbeck M, Alle P, Corfu F, Griffin WL, Meier M, Oberli F, von Quadt A, Roddick JC, Spiegel W (1995) Three natural zircon standards for U–Th–Pb, Lu–Hf, trace element and REE analyses. Geostand Newsl 19: 1–23

Yazdi M (1997) Gold Mineralization in the Granitoid Rocks of the Voltuš area, Rožmitál Block. Unpublished PhD Thesis, Charles University, Prague, pp 1–169

Yazdi M, Košler J, Pertold Z (1997) U–Pb isotope geochronology and geochemical characteristics of the rocks from Voltuš area in the Rožmitál block, Czech Republic. J Czech Geol Soc 42: 77

Zachariáš J, Pertold Z, Pudilová M, Žák K, Pertoldová J, Stein HJ, Markey R (2001) Geology and genesis of Variscan porphyry-style gold mineralization, Petráčkova Hora deposit, Bohemian Massif, Czech Republic. Miner Depos 36: 517–541

Žák J, Holub FV, Verner K (2005a) Tectonic evolution of a continental magmatic arc from transpression in the upper crust to exhumation of mid-crustal orogenic root recorded by episodically emplaced plutons: the Central Bohemian Plutonic Complex (Bohemian Massif). Int J Earth Sci 94: 385–400

Žák J, Schulmann K, Hrouda F (2005b) Multiple magmatic fabrics in the Sázava Pluton (Bohemian Massif, Czech Republic): a result of superposition of wrench-dominated regional transpression on final emplacement. J Struct Geol 27: 805–822

Žák J, Dragoun F, Verner K, Chlupáčová M, Holub FV, Kachlík V (2009) Forearc deformation and strain partitioning during growth of a continental magmatic arc: the northwestern margin of the Central Bohemian Plutonic Complex, Bohemian Massif. Tectonophysics 469: 93–111

Žák J, Kratinová Z, Trubač J, Janoušek V, Sláma J, Mrlina J (2010) Structure, emplacement, and tectonic setting of Late Devonian granitoid plutons in the Teplá–Barrandian Unit, Bohemian Massif. Int J Earth Sci 100: 1477–1495

Žák K, Dobeš P (1991) Stable isotopes and fluid inclusions in hydrothermal deposits: the Příbram ore region. Rozpr Čs Akad Věd, Ř mat přír Věd, Academia, Prague, pp 1–109

Žák K, Vlašímský P, Snee LW (1998) $^{40}Ar/^{39}Ar$ cooling ages of selected rocks of the Příbram ore region and the question of timing of sulfidic hydrothermal mineralization. Zpr geol výzk v r 1997: 172–173 (in Czech)